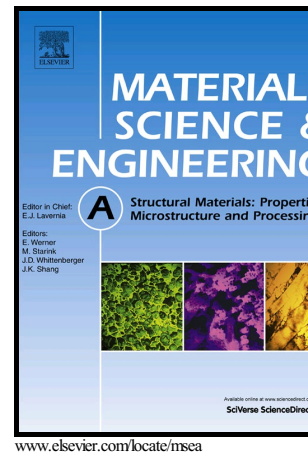# Author's Accepted Manuscript

Effect of grain size on compressive behaviour of titanium at different strain rates

Shixiong Zhang, Ying Chun Wang, Alexander P. Zhilyaev, Elena Korznikova, Shukui Li, Georgy I. Raab, Terence G. Langdon

Cite this article as: Shixiong Zhang, Ying Chun Wang, Alexander P. Zhilyaev, Elena Korznikova, Shukui Li, Georgy I. Raab and Terence G. Langdon, Effec of grain size on compressive behaviour of titanium at different strain rates *Materials   Science   &   Engineering   A* http://dx.doi.org/10.1016/j.msea.2015.08.031

Effect of grain size on compressive behaviour of titanium

at different strain rates

Shixiong Zhang [a], Ying Chun Wang [a*], Alexander P. Zhilyaev [b,c], Elena Korznikova [b], Shukui Li [a], Georgy I. Raab [d], Terence G. Langdon [e]

[a] School of Materials Science and Engineering, Beijing Institute of Technology, Beijing 100081, China

[b] Institute for Problems of Metals Superplasticity, Russian Academy of Sciences, Khalturina 39, Ufa 450001, Russia

[c] Research Laboratory for Mechanics of New Nanomaterials, St. Petersburg State Polytechnical University, Polytechnicheskaya 29, St. Petersburg 195251, Russia

[d] Institute of Physics of Advanced Materials, Ufa State Aviation Technical University, 12 K. Marx Street, Ufa 450000, Russia

[e] Materials Research Group, Faculty of Engineering and the Environment, University of Southampton, Southampton SO17 1BJ, UK

Abstract:

An investigation was conducted to evaluate the dependence on grain size of the compressive deformation of commercial purity (CP) Ti. Tests were performed at room temperature using grain sizes from coarse-grained CG (20 μm) to ultrafine-grained UFG (500 nm) and nanocrystalline NC (90 nm) with testing strain rates in the range from 0.01 to 10 s^{-1}. The results show the flow stress and the strain rate sensitivity of CP Ti increase with decreasing grain size. Work hardening dominates at all strain rates in CG Ti but it balances with flow softening at 0.01 and 0.1 s^{-1} in UFG and NC Ti and there is obvious flow softening in these two materials at 10 s^{-1}.

[*]Corresponding author: Ying Chun Wang, e-mail: wangyc@bit.edu.cn,
Tel:+8610-68913937-801

1. Introduction

Commercial purity (CP) Ti is used extensively for medical implants and as a structural metal for high-performance applications due to its excellent biocompatibility and good corrosion resistance [1]. Nevertheless, coarse-grained (CG) CP Ti has limited strength which is not capable of fully meeting the requirements for medical implants. An effective solution to minimize this disadvantage is to produce ultrafine-grained (UFG) or nanocrystalline (NC) CP Ti having grain sizes in the submicrometer or nanometer ranges. Processing through the application of severe plastic deformation (SPD) is now widely used for producing bulk UFG/NC materials [2-4]. Several SPD techniques are currently available but one of the most attractive is equal-channel angular pressing (ECAP) in which a material is pressed through a die constrained within a channel bent through an abrupt angle [5]. Previous studies showed that UFG/NC Ti achieved by ECAP or a combination of ECAP with traditional plastic deformation exhibits greatly enhanced strength and other improved properties by comparison with the CG materials [6-12]. Thus, it is apparent that the grain size is a major factor influencing the mechanical properties of CP Ti.

Extensive results are now available describing the dependence of grain size on the mechanical properties over a range of strain rates, such as the strain rate sensitivity and the transition from work hardening to flow softening, for pure metals such as Ni, Al and Mg and their alloys having fine-grained microstructures [13-19]. For pure Ti, it was reported that there is a significantly enhanced tensile strength and hardness and improved fatigue and micro-tribological behavior when comparing UFG Ti with CG Ti [20-33]. For example, refinement of Ti to 150 nm in grain size leads to a significant increase of its mechanical

1

strength such that the yield strength increases up to 1190 MPa and the ultimate tensile strength up to 1230 MPa[25]. However, the corresponding data for CP Ti when testing under compressive conditions at various strain rates is not currently available. Such data for CP Ti may be considered as a first step for further investigations of the mechanical response and for providing the basic properties to facilitate the use of CP Ti under a range of different loading conditions. Thus, the objective of the present research was to study the effect of grain size on the compressive behavior of CP Ti by testing with different grain sizes over a range of strain rates from 0.01 to 10 s^{-1}. Details of the deformed microstructures were also investigated after compressive testing in order to clarify the stability of the ultrafine-grained structures

2. Experimental material and procedures

The commercial material used in this study was a forged CP Ti (grade 2) rod with a chemical composition (in wt.%) of C 0.01, Fe 0.09, H 0.001, N 0.01, O 0.13 and with Ti as the balance. The material was annealed at 700°C for 1 h and cooled in air to stabilize the microstructure and remove all residual stresses. With this procedure, an equiaxed microstructure was obtained with an average coarse grain size of ~20 μm as shown in Fig. 1. This condition is henceforth designated CG Ti.

To obtain a UFG microstructure, a billet cut from the annealed CP Ti rod was processed using ECAP at room temperature for 2 passes and then at 275°C for 6 passes using processing route B_C in which the billet is rotated by 90° in the same direction between each pass [34]. The ECAP facility contained an abrupt abutment where the billet was forced through an angle of 90° into the exit channel thereby introducing a strain of ~1 for each separate pass [35].

Typical microstructures observed after processing by transmission electron microscopy (TEM), together with the associated diffraction patterns, are shown in Fig. 2 for (a) a transverse section and (b) a longitudinal section of the billet. On the transverse section in Fig. 2(a) there are reasonably equaxied grains with straight boundaries and having an average size of ~500 nm. The subgrains formed by dislocations interactions in the interiors of the grains had low boundary misorientations as confirmed by the diffraction patterns. On the longitudinal section in Fig. 2(b) there is a banded structures with elongated grains having widths of ~300-400 μm and sets of tangled dislocations, dislocation clusters and subgrains distributed within the grains. Thus, a UFG Ti with a grain size of ~500 nm was used in this investigation.

In an attempt to obtain a nanometer grain size in the CP Ti, another billet was subjected to a two-step processing by combining ECAP-Conform [36,37] and drawing. More details about this processing and the microstructures were given earlier [38,39] and the procedure produced a nanocrystalline CP Ti with an average grain size of ~90 nm in the transverse section.   This was used in this investigation as an NC Ti.

Compressive cylindrical specimens having three different grain sizes were cut from the bar after annealing, the billet processed by ECAP and the billet processed by ECAP-Conform and drawing. These specimens had diameters of 5 mm and heights of 5 mm with the longitudinal axes oriented parallel to the axial directions. All compressive testing was undertaken at room temperature using a Universal testing machine and a Gleeble 3500 thermal simulator with initial strain rates of 0.01, 0.1, 1.0 and 10 s^{-1}. The microstructures were examined on the longitudinal sections after compression at 0.01 and 10 s^{-1} using a

JEM-2100 LaB$_6$ TEM operating at 100 kV. Thin foils of the cross-sectional areas were prepared by mechanical grinding using grit papers with different particle sizes from 800 to 2000 mesh and then thinning to electron transparency using a Gatan Dual Ion Milling System.

3. Experimental results

3.1 Stress-strain behavior

Fig. 3 illustrates the true stress-true strain curves for CP Ti having different grain sizes tested in compression at room temperature over strain rates of (a) 0.01 s^{-1}, (b) 0.1 s^{-1}. (c) 1 s^{-1} and (d) 10 s^{-1}: the grain sizes in Fig. 3 are designated as CG (~20 μm), UFG (~500 nm) and NC (~90 nm).

It is readily apparent from Fig. 3 that the flow stress behavior is strongly influenced by the grain size so that, with a refinement in grain size from 20 μm to 90 nm, the flow stress increases significantly at these four strain rates. For example, in Fig.3(a) at 0.01 s^{-1} the values of the yield stresses, $\sigma_{0.2}$, are ~250 MPa for CG Ti, ~580 MPa for UFG Ti and ~780 MPa for NC Ti. For the highest stain rate of 10 s^{-1}, the yield stress values are ~510, ~900, ~1310 MPa, respectively. This demonstrates that UFG and NC structures are very advantageous for improving the strength of the titanium without the introduction of any alloying elements. Furthermore, the stress levels attained are appropriate for applications in medical devices so that the CP Ti becomes suitable for use in a wide range of applications.

A comparison of Fig. 3(a)-(d) provides information on the nature of the strain rate sensitivity of the CP Ti in testing at room temperature. At this temperature, the flow stress increases with increasing strain rate for all grain sizes but there are differences in behavior for

the various grain sizes. Thus, for CG Ti the change in yield stress between 0.01 and 10 s^{-1} is ~260 MPa whereas there are larger changes of ~320 MPa for UFG Ti and ~530 MPa for NC Ti. These results show that the strain rate sensitivity of the flow stress increases with decreasing grain size.

It is also apparent from Fig. 3 that at strain rates of 0.01 and 0.1s^{-1} the flow stress of CG increases continuously with increasing strain until unloading, thereby showing that work hardening plays a dominant role throughout the deformation. By contrast, the increase for UFG and NC Ti is not obvious which indicates the work hardening effect is weakened in SPD-processed Ti. In Fig.3(c) at a strain rate of 1 s^{-1}, the flow stress of CG Ti increases continuously with increasing strain whereas in UFG and NC Ti there is a short period where the true stress increases slowly to a peak value and thereafter the stress remains essentially constant. This steady-state condition shows that the flow softening is essentially balanced by the strain hardening throughout most of the deformation. In Fig. 3(d) for a strain rate of 10 s^{-1}, flow softening prevails over the deformation behavior of UFG and NC Ti whereas work hardening is dominant in the CG Ti.

3.2 Microstructures after compression

Typical microstructures of CP Ti after compression are shown in Fig. 4 for samples tested at room temperature using strain rates of 0.01 and 10 s^{-1} where the three columns refer to CG, UFG and NC Ti, respectively. Inspection of Fig. 4(a) shows that the initial coarse equiaxed grains evolve to reasonably elongated grains due to the compression, and there is an abundance of dislocation clusters and tangled dislocations within the grain interiors. Similarly, in Fig. 4(d) after compression at 10 s^{-1} the microstructure of the CG Ti is similar to Fig. 4(a)

with a very high density of dislocations.

The microstructure of UFG Ti compressed at 0.01 s^{-1} is shown in Fig. 4(b) and it is readily apparent that the initial grain boundaries are now less distinct, there is again a high dislocation density, very small subgrains are present within the grains and there is evidence for the emergence of new grains. The diffraction pattern of Fig. 4(b) contains rings of diffraction spots suggesting that many of the grain boundaries have high angles of misorientation but the rings are discontinuous and some of the spots remain clustered which confirms the existence of some low-angle boundaries. The presence of diffuse boundaries between highly deformed grains is consistent with very early reports of the microstructures produced in an aluminum alloy after processing by ECAP [40]. In Fig. 4(e) after compression of UFG Ti at 10 s^{-1}, the elongated grains visible in Fig. 2(b) are no longer present but instead there are essentially equiaxed grains with an average size of ~100 nm. The corresponding diffraction pattern shows a more uniformly continuous distribution of diffraction images by comparison with Fig. 4(b) where the spots form almost continuous rings indicating the presence of a high volume of high-angle grain boundaries. These results show, therefore, that the grains become more equiaxed with increasing strain rate from 0.01 to 10 s^{-1}.

The TEM image of NC Ti compressed at 0.01 s^{-1} in Fig. 4(c) shows again that the initial elongated grains are replaced by equiaxed grains having an average size of ~30 nm. The corresponding diffraction pattern shows most of these boundaries have high angles of misorientation. At the higher strain rate of 10 s^{-1} in Fig. 4(f), there is a homogeneous distribution of equiaxed grains with an average size of ~50 nm and with the diffraction pattern confirming the presence of high-angle grain boundaries.

6

4. Discussion

4.1 Microstructural stability during compression

The appearance of new equiaxed grains in Fig. 4(b), (c), (e) and (f) suggests the initiation of dynamic recrystallization (DRX) when UFG Ti and NC Ti are compressed at strain rates of 0.01 to 10 s^{-1} whereas there is no DRX at these strain rates during the compression of CG Ti. From these results it is concluded that, as a consequence of the very small grain sizes, SPD-processed Ti shows a decreasing stability of structure when it is subjected to additional plastic deformation. It is well known that SPD processing may lead to an enhanced interfacial energy due to grain refinement and the development of long-range internal stresses [42-44] that may contribute to an inherent microstructural instability.

In addition, when materials are processed by SPD and then subjected to further deformation, microstructural evolution may occur through DRX or dynamic recovery (DRV). It was noted earlier that the DRX mechanism for NC Ti subjected to dynamic deformation at low strain rates corresponds to the classic migration dynamic recrystallization (m-DRX) in which the pre-existing high-angle boundaries migrate through the deformed structure to leave strain-free regions [38,41,42].

4.2 Strain rate sensitivity

The effect of strain rate on the mechanical behaviour of CP Ti having different grain sizes can be described further by analyzing the variation of the flow stress as a function of strain and strain rate.

Fig. 5(a) and (b) show the variation of true stress with strain rate plotted in a semi-logarithmic form with the stress measured at a strain, ε, of (a) 0.1 and (b) 0.2 for the CG,

UFG and NC Ti tested in compression at room temperature. For both of these strains, the flow stress increases with increasing strain rate and the curves depict well-defined linear segments where the slopes are different for each grain size thereby showing that the strain rate sensitivity is related to the strain rate.

To quantitatively analyze the sensitivity of the flow stress to the strain rate, the strain rate sensitivity, m, is determined at a constant strain and temperature using the relationship given by [43]:

$$m = \frac{\log(\sigma_1/\sigma_2)}{\log(\dot{\varepsilon}_1/\dot{\varepsilon}_2)}\bigg|\varepsilon \qquad (1)$$

where the subscripts 1 and 2 denote two separate conditions of stress and strain rate. For convenience, the values calculated for m are also given in Fig. 5. It is readily apparent that the calculated values of m tend to increase with decreasing grain size at the four testing strain rates of 0.01, 0.1, 1 and 10 s^{-1} and at both of the selected strains shown in Fig. 5. This is reasonable because of the relationship between m and the apparent activation volume, V^*[44] which is given by:

$$m = \frac{MkT}{\sigma V^*} \qquad (2)$$

where M is the Taylor factor, k is the Boltzmann constant and T is the absolute temperature.

The value of V^* can be described in terms of the number of atoms involved in the thermal activation event of the moving dislocation overcoming localized obstacles along the slip planes. An equation for the activation volume may be proposed based on a microscopic physical model of dislocation movement as given by [45]:

$$V^* = b \times \xi \times l^* \qquad (3)$$

where b is the Burgers vector of the dislocations，ξ is the average distance swept out by a

8

mobile dislocation during a single activation event and l^* is the length of the dislocation segment involved in the thermal activation. It has been demonstrated that dislocation motion and the value of the activation volume both vary with grain size during plastic deformation [46] and for CP Ti the magnitudes of V^* were estimated as $\sim276b^3$, $\sim57b^3$ and $\sim5b^3$ for CG, UFG and NC Ti, respectively [47]. Although a reduction in grain size gives rise to an enhancement in stress, nevertheless this rise becomes less important when considering the drastic increase in the dislocation density in the coarser grains so that an increase in m with decrease in grain size is observed in the CP Ti. Finally, a comparison of Fig. 5 (a) and (b) also shows lower values of m when ε increases from 0.1 to 0.2 in addition to when the stress rises. A similar trend of m decreasing with increasing σ was also reported in studies on UFG Ni [47], Cu [48] and an Al-1.5% Mg alloy [49].

4.3 Work hardening and flow softening

The apparent increasing flow stress with strain in CG Ti as shown in Fig. 3 demonstrates the presence of work hardening in the deformation of CG Ti at all strain rates from 0.01 to 10 s^{-1} and this suggests that there is an abundance of dislocations participating in the deformation as suggested by the microstructures in Fig. 4(a) and (d). Regarding UFG and NC Ti, the flow stresses after yielding tend to be steady or even to decline.

The absence of work hardening is an important characteristic of the deformation behavior of SPD-processed materials [50]. Thus, after SPD processing the work hardening capacity is almost exhausted. The refinement of the originally large grains is achieved through the accumulation and rearrangement of the dislocations generated during SPD processing. These materials are characterized by heavy deformation microstructures, where

9

the density of dislocations becomes high or even saturated. Nevertheless, the observation of new dislocation-free grains by TEM, as shown in Fig. 4, reveals the process of dynamic recovery and DRX in which most of the dislocations are absorbed by the grain boundaries. Thus, this leads to a lack of dislocation accumulation and relatively insignificant work hardening.

It is generally considered that flow softening may occur in pure Ti and its alloys when deformed at high strain rates due to the low thermal conductivity of these materials [51]. For the UFG and NC Ti at 0.01 and 0.1 s^{-1}, the flow softening is not strong and it almost balances with the work hardening in the deformation of the SPD-processed Ti in Fig. 3 (a) and (b). With increasing strain rate up to 1 s^{-1}, however, flow softening then plays a crucial role. The reason for such a difference in the compressive behavior of UFG and NC Ti lies in the value of the adiabatic temperature that serves to accelerate the flow softening.

The adiabatic temperature rise during dynamic deformation may be calculated by the following relationship [52]:

$$\Delta T = \frac{\beta}{\rho C_p} \int_0^{\varepsilon_f} \sigma \cdot d\varepsilon \qquad (4)$$

where β is the Taylor-Quinney coefficient characterizing the portion of plastic work converted into heat, ρ is the density of the material, C_p is the specific heat, σ is the flow stress and ε_f is the true fracture strain. Typically, direct experimental measurements showed that the temperature may rise by ~70 K in a high strength aluminum alloy when processing by ECAP [57] and this was subsequently confirmed using finite element modeling [58] and a heat transfer analysis [59].

It follows from Eq. (4) that more heat is generated from the adiabatic temperature with

increasing flow stress which, from Fig. 3, clearly increases with increasing strain rate. Thus, the increasing adiabatic temperature strengthens the flow softening by accelerating the process of DRV and DRX with both increasing strain rate and decreasing grain size. In addition, an elevated temperature will increase the thermal activation energy of CP Ti and the average kinetic energy of the atoms, thereby decreasing the critical shear for crystal slip and weakening the obstacles for dislocation movement [53]. As a result, and as shown in Fig. 3, the flow stress remains reasonably steady or decreases instead of increasing for both UFG and NC Ti.

5. Summary and conclusions

1. Experiments were conducted on commercial purity (CP) Ti to examine the effect of grain size in the range of ~90 nm to ~20 μm on the microstructural evolution and compressive behavior over a range of strain rates from 0.01 to 10 s^{-1} at room temperature.

2. For CP Ti with grain sizes from ~90 nm to ~20 μm, the flow stress increases with decreasing grain size and increasing strain rate from 0.01 to 10 s^{-1}. The strain rate sensitivity increases with decreasing grain size due to a decrease in the apparent activation volume which is attributed to the very high dislocation density in the grain-refined microstructure.

3. Work hardening accounts for all of the compressive deformation in CG Ti from 0.01 to 10 s^{-1}. However, it essentially balances with flow softening in the compression of UFG and NC Ti at 0.01~0.1 s^{-1} but the effect of flow softening becomes apparent at strain rates of 1 to 10 s^{-1}.

4. The operation of migration dynamic recrystallization (m-DRX) in UFG and NC Ti demonstrates a decreasing microstructural stability which is due to the significant grain

11

refinement introduced by ECAP processing.

Acknowledgements

References

[1] S. Ferraris, A.Venturello, M.Miolaa, A.Cochis, L.Rimondini, S.Spriano. Antibacterial and bioactive nanostructured titanium surfaces for bone integration, App. Surf. Sci. 311 (2014) 279-291.

[2] R.Z. Valiev, R.K. Islamgaliev, I.V. Alexandrov. Bulk nanostructured materials from severe plastic deformation. Prog. Mater. Sci. 45 (2000):103-189

[3] C.P. Wang, F.G. Li, B. Chen, Z.W. Yuan, H.Y. Lu, Severe plastic deformation techniques for bulk ultrafine-grained materials, Rare Metal Mater. Eng. 41 (2012) 0941-0946.

[4] T.G. Langdon, Tweinty-five years of ultrafine-grained materials: Achieving exceptional properties through grain refinement, Acta Mater. 61 (2013) 7035-7059.

[5] R.Z. Valiev, T.G. Langdon, Principles of equal-channel angular pressing as a processing tool for grain refinement. Prog. Mater. Sci. 51(2006):881-981

[6] V.V. Stolyarov, Y.T. Zhu, T.C. Lowe, R.Z. Valiev, Microstructure and properties of pure Ti processed by ECAP and cold extrusion, Mater. Sci. Eng. A 303 (2001) 82 -89.

[7] V.V. Stolyarov, Y.T. Zhu, I.V. Alexandrov, T.C. Lowe, R.Z. Valiev, Grain refinement and properties of pure Ti processed by warm ECAP and cold rolling, Mater. Sci. Eng. A 343 (2003) 43-50.

[8] V.V. Stolyarov, L.Sh. Shuster, M.Sh. Migranov, R.Z. Valiev, Y.T. Zhu, Reduction of friction coefficient of ultrafine-grained CP titanium, Mater. Sci. Eng. A 371 (2004) 313-317.

[9] X.C. Zhao, X.R. Yang, X.Y. Liu, X.Y. Wang, T.G. Langdon, The processing of pure titanium through multiple passes of ECAP at room temperature, Mater. Sci. Eng. A 527 (2010) 6335-6339.

[10] Y. Zhang, R.B. Figueiredo, S.N. Alhajeri, J.T. Wang, N. Gao, T.G. Langdon, Structure and mechanical properties of commercial purity titanium processed by ECAP at room temperature, Mater. Sci. Eng. A 528 (2011) 7708-7714.

[11] V.L. Sordi, M. Ferrante, M. Kawasaki, T.G. Langdon, Microstructure and tensile strength of grade 2 titanium processed by equal-channel angular pressing and by rolling, J. Mater. Sci. 47 (2012) 7870-7876.

[12] L. Wang, Y.C. Wang, A.P. Zhilyaev, A.V. Korznikov, S.K. Li, E. Korznikova, T.G. Langdon, Microstructure and texture evolution in ultrafine-grained pure Ti processed by equal-channel angular pressing with subsequent dynamic compression, Scripta Mater. 77 (2014) 33-36.

[13] K.D. Woo, S.W. Kim, C.H. Yanga, T.P. Lou, Y. Miura, Effects of grain size on high temperature deformation behavior of Al-4Mg-0.4Sc alloy, Mater. Lett. 57 (2003) 1903-1909.

[14] J.A. del Valle, O.A. Ruano, Influence of the grain size on the strain rate sensitivity in an Mg-Al-Zn alloy at moderate temperatures, Scripta Mater. 55 (2006) 775-778.

[15] X.L. Wu, E. Ma, Dislocations and twins in nanocrystalline Ni after severe plastic deformation: the effects of grain size, Mater. Sci. Eng. A 483-484 (2008) 84-86.

[16] J.Z. Li, W. Xu, X.L. Wu, H. Ding, K.N. Xia, Effects of grain size on compressive behaviour in ultrafine grained pure Mg processed by equal channel angular pressing at room temperature, Mater. Sci. Eng. A 528 (2011) 5993-5998.

[17] L.L. Guo, Z.C. Chen, L. Gao, Effects of grain size, texture and twinning on mechanical properties and work-hardening behavior of AZ31 magnesium alloys, Mater. Sci. Eng. A 528 (2011) 8537-8545

[18] Y.D. Qiao, X.Wu, Z.Y. Liu, E. Wang, Effects of grain size, texture and twinning on mechanical properties and work-hardening behaviors of pure Mg, Mater. Sci. Eng. A 578 (2013) 240-246.

[19] H.Y. Wang, E.S. Xue, X.L. Nan, T. Yue, Y.P. Wang, Q.C. Jiang, Influence of grain size on strain rate sensitivity in rolled Mg-3Al-3Sn alloy at room temperature, Scripta Mater. 68 (2013) 229-232.

[20] V. V. Stolyarov, Y. T. Zhu, I.V. Alexandrov, T. C. Lowe, R. Z. Valiev, Grain refinement and properties of pure Ti processed by warm ECAP and cold rolling, Mater. Sci. Eng. A343 (2003) 43-50.

[21] I. P. Semenova, R. Z. Valiev, E. B. Yakushina , G. H. Salimgareeva, T. C. Lowe, Strength and fatigue properties enhancement in ultrafine-grained Ti produced by severe plastic deformation, J. Mater. Sci. 43 (2008) 7354-7359.

[22] G. Purcek, O. Saray, O. Kul, I. Karaman, G.G. Yapici, M. Haouaoui, H.J. Maier, Mechanical and wear properties of ultrafine-grained pure Ti produced by multi-pass equal-channel angular extrusion, Mater. Sci. Eng. A 517 (2009) 97-104.

[23] I. Sabirov, M.T. Perez-Prado, J.M. Molina-Aldareguia, I.P. Semenova, G.K. Salimgareeva, R.Z. Valiev, Anisotropy of mechanical properties in high-strength ultra-fine-grained pure Ti processed via a complex severe plastic deformation route, Scripta Mater. 64 (2011) 69-72.

[24] C.T. Wang, N. Gao, M.G. Gee, R.J.K. Wood, T. G. Langdon, Effect of grain size on the micro-tribological behavior of pure titanium processed by high-pressure torsion, Wear 280-281 (2012) 28-35.

[25] D.V. Gunderov, A.V. Polyakov, I.P. Semenova, G.I. Raab, A.A. Churakova, E.I. Gimaltdinova, I. Sabirov, J. Sagurado, V.D. Sitdikov, I.V. Alexandrov, N.A. Enikeev, R.Z. Valiev, Evolution of microstructure, macrotexture and mechanical properties of commercially pure Ti during ECAP-conform processing and drawing, Mater. Sci. Eng. A 562 (2013) 128-136.

[26] C.N. Elias, M.A. Meyers, R.Z. Valiev, S.N. Monteiro, Ultrafine grained titanium for biomedical applications:An overview of performance, J. Mater. Res. Technol. 2 (2013) 340-350

[27] C.T. Wang, N. Gao, M.G. Gee, R.J.K. Wood, T.G. Langdon, Tribology testing of ultrafine-grained Ti processed by high-pressure torsion with subsequent coating, J. Mater. Sci. 48 (2013) 4742-4748.

[28] A.V. Polyakov, I.P. Semenova, R.Z. Valiev, Y. Huang, T.G. Langdon, Influence of annealing on ductility of ultrafine-grained titanium processed by equal-channel angular pressing-Conform and drawing, MRS Comm. 3 (2013) 249-253.

[29] C.T. Wang, N. Gao, M.G. Gee, R.J.K. Wood, T.G. Langdon, Processing of an ultrafine-grained titanium by high-pressure torsion: An evaluation of the wear properties with and without a TiN coating, J. Mech. Behav. Biomed. Mater. 17 (2013) 166-175.

[30] C.T. Wang, A. Escudeiro, T. Polcar, A. Cavaleiro, R.J.K. Wood, N. Gao, T.G. Langdon, Indentation and scratch testing of DLC-Zr coatings on ultrafine-grained titanium processed by high-pressure torsion, Wear 306 (2013) 304-310.

[31] X. Zhao, X. Yang, X. Lin, C.T. Wang, Y. Huang, T.G. Langdon, Processing of commercial purity titanium by ECAP using a 90 degrees die at room temperature, Mater. Sci.

Eng. A607 (2014) 482-489

[32] M. Shirooyeh, J. Xu, T.G. Langdon, Microhardness evolution and mechanical characteristics of commercial purity titanium processed by high-pressure torsion, Mater. Sci. Eng. A614 (2014) 223-231.

[33] M. Nie, C.T. Wang, M. Qu, N. Gao, J.A. Wharton, T.G. Langdon, The corrosion behaviour of commercial purity titanium processed by high-pressure torsion, J. Mater. Sci. 49 (2014) 2824-2831.

[34] C.T. Wang, A.G. Fox, T.G. Langdon, Microstructural evolution in ulrtafine-grained titanium processed by high-pressure torsion under different pressures, J. Mater. Sci. 49 (2014) 6558-6564.

[35] M. Furukawa, Y. Iwahashi, Z. Horita, M. Nemoto, T.G. Langdon, The Shearing Characteristics Associated with Equal-Channel Angular Pressing, Mater. Sci. Eng. A257 (1998) 328-332.

[36] Y. Iwahashi, J. Wang, Z. Horita, M. Nemoto, T.G. Langdon, Principle of Equal-Channel Angular Pressing for the Processing of Ultrafine-Grained Materials, Scripta Mater. 35 (1996) 143-146.

[37] G.J. Raab, R.Z. Valiev, T.C. Lowe, Y.T. Zhu, Continuous Processing of Ultrafine Grained Al by ECAP-Conform, Mater. Sci. Eng. A382 (2004) 30-34.

[38] C. Xu, S. Schroeder, P.B. Berbon, T.G. Langdon, Principles of ECAP-Conform as a Continuous Process for Achieving Grain Refinement: Application to an Aluminum Alloy, Acta Mater. 58 (2010) 1379-1386.

[39] S.X. Zhang, Y. C. Wang, A.P. Zhilyaev, D.V. Gunderov, S.K. Li, G.I. Raab, E.

Korznikova, T.G. Langdon, Effect of temperature on microstructural stabilization and mechanical properties in the dynamic testing of nanocrystalline pure Ti, Mater. Sci. Eng. A 634 (2015) 64-70.

[40] S.X. Zhang, Y. C. Wang, A.P. Zhilyaev, E. Korznikova, S.K. Li, G.I. Raab, T.G. Langdon, Temperature and strain rate dependence of microstructural evolution and dynamic mechanical behavior in nanocrystalline Ti, Mater. Sci. Eng. A 641 (2015) 29-36.

[41] J. Wang, Z. Horita, M. Furukawa, M. Nemoto, N.K. Tsenev, R.Z. Valiev, Y. Ma, T.G. Langdon, An investigation of ductility and microstructural evolution in an Al-3% Mg alloy with submicron grain size, J. Mater. Res. 8 (1993) 2810-2818.

[42] S.N. Alhajeri, A.G. Fox, T.G. Langdon, A convergent-beam electron diffraction study of strain homogeneity in severely strained aluminum processed by equal-channel angular pressing, Acta Mater. 59 (2011) 7388-7395.

[43] I.F. Lee, T.Q. Phan, L.E. Levine, J.Z. Tischler, P.T. Geantil, Y. Huang, T.G. Langdon, M.E. Kassner, Using X-ray microbeam diffraction to study the long-range internal stresses in aluminum processed by ECAP, Acta Mater. 61 (2013) 7741-7748.

[44] T.Q. Phan, I.F. Lee, L.E. Levine, J.Z. Tischler, Y. Huang, A.G. Fox, T.G. Langdon, M.E. Kassner, X-ray microbeam measurements of long-range internal stresses in commercial-purity aluminum processed by multiple passes of equal-channel angular pressing, Scripta Mater. 93 (2014) 48-51.

[45] M.R. Barnett, A practical condition for migration dynamic recrystallization, Acta Mater. 55 (2007) 3271-3278.

[46] S.Wu, K.Fan, P. Jiang, S. Chen, Grain refinement of pure Ti during plastic deformation,

Mater. Sci. Eng. A 527 (2010) 6917-6921.

[47] D.V. Gunderov, G. Maksutova, A. Churakova, A. Lukyanov, A. Kreitcberg, G.I. Raab, I. Sabirov, S. Prokoshkin, Strain rate sensitivity and deformation activation volume of coarse-grained and ultrafine-grained TiNi alloys, Scripta Mater. 102 (2015) 99-102.

[48] R. Kapoor, J.B. Singh, J.K. Chakravartty, High strain rate behavior of ultrafine-grained Al-1.5 Mg, Mater. Sci. Eng. A 496 (2008) 308-315.

[49] Q. Wei, S. Cheng, K.T. Ramesh, E. Ma, Effect of nanocrystalline and ultrafine grain sizes on the strain rate sensitivity and activation volume: fcc versus bcc metals, Mater. Sci. Eng. A 381 (2004) 71-79.

[50] F. Wang, B. Li, T.T. Gao, P. Huang, K.W. Xu, T.J. Lu, Activation volume and strain rate sensitivity in plastic deformation of nanocrystalline Ti, Surf. Coat. Tech. 228 (2013) 254-256.

[51] Y.J. Li, X.H. Zeng, W. Blum, Transition from strengthening to softening by grain boundaries in ultrafine-grained Cu, Acta Mater. 52 (2004) 5009-5018.

[52] Y.J. Li, J. Mueller, H.W. Hoppel, M. Goken, W. Blum, Deformation kinetics of nanocrystalline nickel, Acta Mater. 55 (2007) 5708-5717.

[53] R. Kapoor, J.K. Chakravartty, Deformation behavior of an ultrafine-grained Al-Mg alloy produced by equal-channel angular pressing, Acta Mater. 55 (2007) 5408-5418.

[54] Y.G. Ko, D.H.Shin, K.T. Park, C.S. Lee, An analysis of the strain hardening behavior of ultra-fine grain pure titanium, Scripta Mater. 54 (2006) 1785–1789.

[55] Z.J. Pu, K.H. Wu, J. Shi, Development of constitutive relationships for the hot deformation of boron microalloying TiAl-Cr-V alloys, Mater. Sci. Eng. 192/193 (1995) 780-787.

[56] L. Wang, Y.C. Wang, A.P. Zhilyaev, A.V. Korznikov, S.K. Li, E. Korznikova, T.G. Langdon, Dynamic compressive behavior of ultrafine-grained pure Ti at elevated temperatures after processing by ECAP, J. Mater. Sci. 19 (2014) 6640-6647.

[57] D. Yamaguchi, Z. Horita, M. Nemoto, T.G. Langdon, Significance of adiabatic heating in equal-channel angular pressing, Scripta Mater. 41 (1999) 791-796.

[58] Q.X. Pei, B.H. Hu, C. Lu, Y.Y. Wang, A finite element study of the temperature rise during equal channel angular pressing, Scripta Mater. 49 (2003) 303-308.

[59] H.S. Kim, Prediction of temperature rise in equal channel angular pressing, Mater. Trans. 42 (2001) 536-538.

[60] T. Suo, Y.L. Li, K. Xie, F. Zhao, K. S. Zhang, Y.Y. Liu, The effect of temperature on mechanical behavior of ultrafine-grained copper by equal channel angular pressing, Mater. Sci. Eng. A 527 (2010) 5766-5772.

Figure captions

Figure 1. Microstructure of CP Ti bar after annealing.

Figure 2. TEM images and diffraction patterns for a CP Ti billet processed by ECAP (a) in a transverse section and (b) in a longitudinal section.

Figure 3. True stress versus true strain curves for CP Ti compressed at strain rates of (a) 0.01 s^{-1}, (b) 0.1 s^{-1}, (c) 1 s^{-1} and (d) 10 s^{-1}.

Figure 4. Microstructures in the longitudinal sections of specimens with different grain sizes after compressive deformation at two different strain rates

Figure 5. A semi-logarithmic plot of stress against strain rate for CP Ti having three different grain sizes at strains of (a) 0.1 and (b) 0.2.
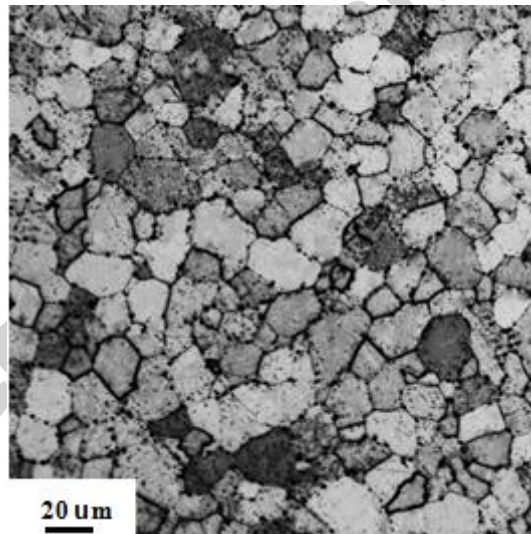

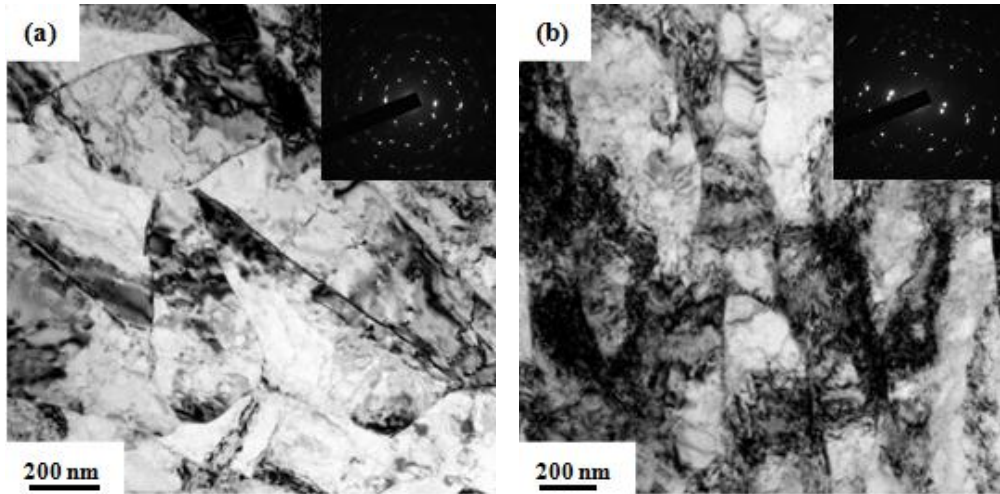Figure 1. Microstructure of CP Ti bar after annealing

Figure 2. TEM images and SAED patterns of a CP Ti billet processed by ECAP (a) in a transverse section and (b) in a longitudinal section.
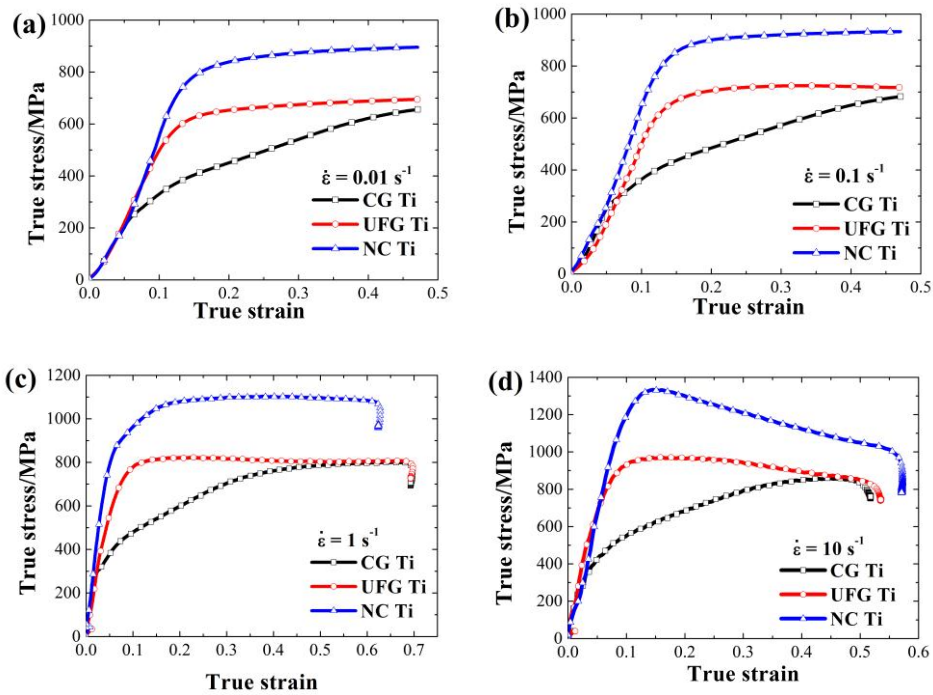

Figure 3. True stress versus true strain curves for CP Ti compressed at strain rates of (a) 0.01 s^{-1}, (b) 0.1 s^{-1}, (c) 1 s^{-1} and (d) 10 s^{-1}

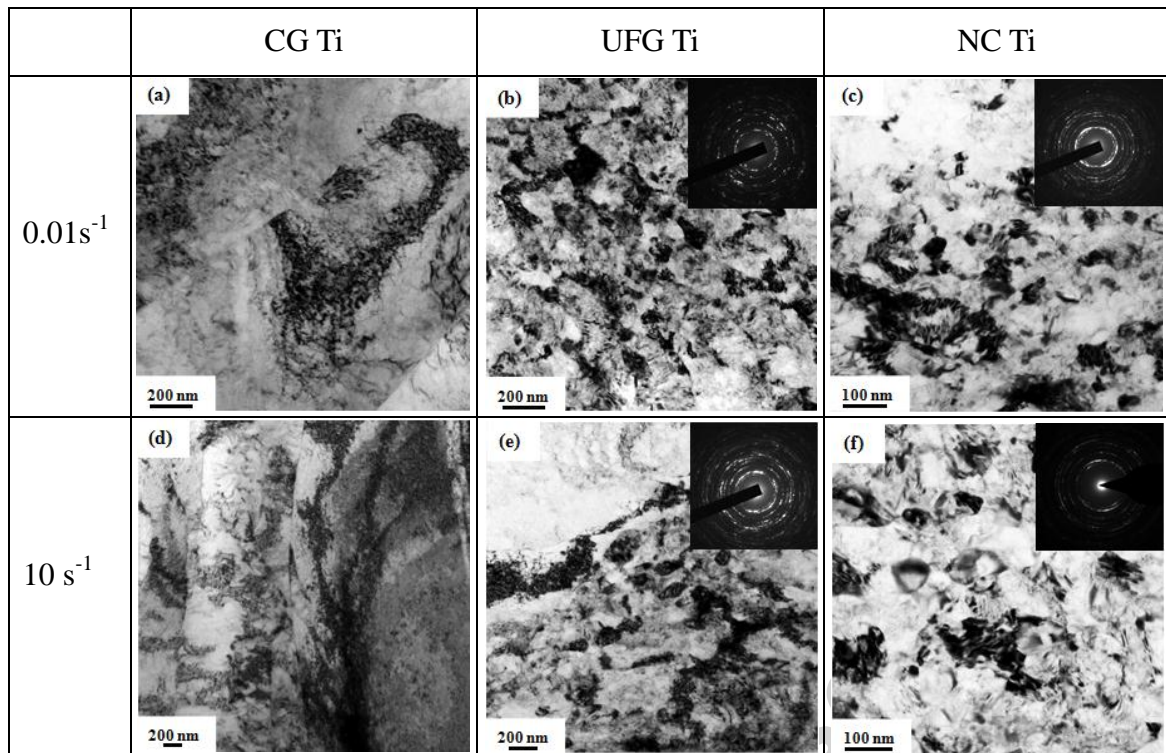|	CG Ti	UFG Ti	NC Ti
0.01s⁻¹			
10 s⁻¹			

Figure 4. Microstructures in the longitudinal sections of specimens with different grain sizes after compressive deformation at two different strain rates
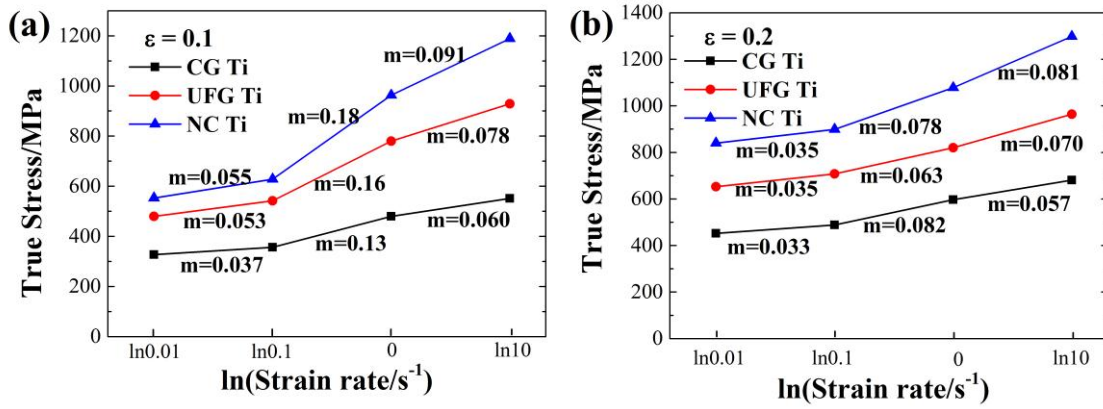
Figure 5. A semi-logarithmic plot of stress against strain rate for CP Ti having three different grain sizes at strains of (a) 0.1 and (b) 0.2